

Enhanced Precision Through Multiple Reads for LDPC Decoding in Flash Memories

Jiadong Wang, Kasra Vakilinia, Tsung-Yi Chen, Thomas Courtade,
Guiqiang Dong, Tong Zhang, Hari Shankar, and Richard Wesel

Abstract—Multiple reads of the same Flash memory cell with distinct word-line voltages provide enhanced precision for LDPC decoding. In this paper, the word-line voltages are optimized by maximizing the mutual information (MI) of the quantized channel. The enhanced precision from a few additional reads allows FER performance to approach that of full precision soft information and enables an LDPC code to significantly outperform a BCH code.

A constant-ratio constraint provides a significant simplification in the optimization with no noticeable loss in performance.

For a well-designed LDPC code, the quantization that maximizes the mutual information also minimizes the frame error rate in our simulations. However, for an example LDPC code with a high error floor caused by small absorbing sets, the MMI quantization does not provide the lowest frame error rate. The best quantization in this case introduces more erasures than would be optimal for the channel MI in order to mitigate the absorbing sets of the poorly designed code.

The paper also identifies a trade-off in LDPC code design when decoding is performed with multiple precision levels; the best code at one level of precision will typically not be the best code at a different level of precision.

Index Terms—Flash Memory, LDPC Codes, Quantization, Mutual Information Maximization, LDPC Decoding, Soft Information, Enhanced Precision

I. INTRODUCTION

Flash memory can store large quantities of data in a small device that has low power consumption and no moving parts. The original NAND Flash uses only two levels. This is called single-level-cell (SLC) Flash because there is only one actively written charge level. Devices currently available using four levels are called multi-level cell (MLC) Flash. Four and eight levels are currently in use, and the number of levels will increase further [1][2].

Error control coding for Flash memory is becoming more important as the storage density increases. The increasing number of levels (and smaller distance between levels) means that variations in cell behavior from cell to cell (and over time due to wear-out) lower the signal-to-noise ratio of the read channel. This makes stronger error-correction codes necessary. Reductions in feature size make inter-cell interference more likely, adding an equalization or interference suppression component to the read channel [3]. Also, the wear-out effect is time-varying, introducing a need for adaptive coding or modulation to maximize the potential of the system.

This work was presented in part at Globecom 2011 in Houston, Texas in December 2011 and at the 2012 Non-Volatile Memories Workshop at UCSD in March of 2012. This research was supported by a gift from Inphi Corp. and UC Discovery Grant 192837.

A. Related Work

Low-density parity-check (LDPC) codes are well-known for their capacity-approaching ability for AWGN channels [4] and are the subject of recent interest for application to the Flash memory read channel. For example, in [5] LDPC codes without access to enhanced precision are shown to provide a performance improvement over BCH codes, but that improvement becomes small at high code rates. Also in [5], an alternative error correction scheme is introduced that takes into account the dominant cell-level errors found in eight-level cells. This scheme provides improvement for eight-level cells without using enhanced precision.

Important work related to codes that consider the dominant cell-level error is the work of Gabrys et al. on graded bit error correcting codes [6]. In contrast to codes designed for dominant errors, our paper focuses on the use of enhanced precision to improve performance. While we explore the improvement in terms of standard LDPC codes, enhanced precision should also improve the performance of alternative error correction schemes that focus on the dominant cell-level errors as long as decoders that support soft information are available.

Another approach for using LDPC codes in Flash memories [7] is to design the codes for use with rank modulation. Rank modulation [8], [9] stores information in the cell using the *relative* value (or ordering) of cell charge levels rather than the absolute value. LDPC codes for Flash memories with rank modulation require the cell charge-level ordering at the decoder.

As observed in [8], rank modulation eliminates the need for discrete cell levels, overcomes overshoot errors when programming cells, and mitigates the problem of asymmetric errors. This is an exciting approach for future Flash architectures. However, current Flash systems use the same word-line voltage to read all cells on the page and thus would require a large number of page reads to learn the charge-level ordering. Our paper focuses on the traditional approach of coding with fixed target charge levels and assumes that when reading each page, the same word-line voltage is used for all cells.

We note that an alternative approach to using multiple reads to enhance precision is to perform a single read but use a dynamic threshold scheme as introduced recently by [10] to adapt to time varying channel degradations such as the mean shift that occurs due to retention loss. We note that the use of dynamic thresholds is complementary to the use

of enhanced precision, and a combined approach could be especially effective.

This paper uses mutual information maximization as the objective function that drives the optimization of the word-line voltages (thresholds) used for the multiple reads that provide enhanced precision. Mutual information maximization is also explored in [11] for the design of memory efficient decoding of LDPC codes and in [12] for quantization of binary-input discrete memoryless channels and the design of the message-passing decoders of LDPC codes used on such channels.

One final aspect of research in Flash memory systems is that current Flash memory systems are designed to erase an entire block of data at once. Each block consists of numerous pages and each page contains thousands of bits. Thus, in order to change data on a single page, the entire block would need to be erased. However, erasing and re-writing data onto a block in order to change a small amount of data degrades performance because each time electrons are written and then erased from the floating gate, the integrity of the floating gate degrades in a process known as “cell wear-out”.

In [13], coding is used to minimize the number block erasures and the number of auxiliary blocks required for moving pages of data in a Flash memory system. Efficient wear-leveling and data movement in Flash is an important problem, but our paper addresses the complementary problem of improving the ability to reliably read a page by using enhanced precision.

B. Overview and Contributions

LDPC codes have typically been decoded with soft reliability information (a real or complex number representing a received symbol value) while Flash memory systems have typically provided only hard reliability information (a single bit representing the output of a sense-amp comparator) to their decoders. This paper demonstrates that a capability for enhanced precision through multiple reads is crucial to successfully reaping the benefits of LDPC coding in Flash memory. The paper explores how to select the word-line voltages used for additional reads, how many such reads are necessary to provide most of the LDPC performance benefit, and how varying levels of precision can impact code design.

Section II briefly introduces the NAND Flash memory model and LDPC codes. Section III shows how to obtain word-line voltages by maximizing the mutual information (MI) of the equivalent read channel using a simple Gaussian model of SLC (two-level) Flash as an example. This section also shows that a few additional reads provide most of the benefit of enhanced precision.

Section IV describes the LDPC codes used in the paper in detail. This section also demonstrates a code design trade-off: the best code in terms of both density evolution threshold [4] and empirical performance at one precision level is not the best according to either density evolution threshold and empirical performance at another precision level. This is a practically important issue because the same code may well be decoded with varying levels of precision. Time will be spent

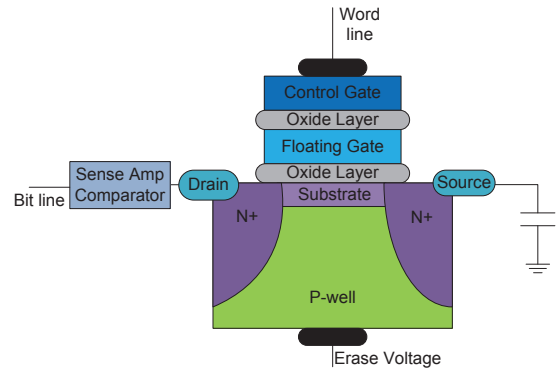


Fig. 1. A NAND Flash memory cell.

on additional page reads to enhance precision only if the page could not be decoded without them.

Section V extends the discussion to MLC (four-level) Flash. This section uses a more realistic model of the Flash read channel from [14] and employs the “constant-ratio” method of [15] as a constraint to simplify the threshold optimization. This section confirms that maximizing mutual information also minimizes frame error rate for a well-designed LDPC code. However, this section also provides an example of a poorly-designed LDPC code where maximizing mutual information does not minimize frame error rate. In this example, larger erasure regions than would maximize the mutual information are needed to mitigate small absorbing sets. The section concludes by presenting simulation results for these two LDPC codes using the channel model of [15]. Section VI delivers the conclusions.

II. BACKGROUND

This section introduces the basics of NAND Flash memory and LDPC codes.

A. Basics of NAND Flash Memory

This paper focuses on the NAND architecture for Flash memory. Fig. 1 shows the configuration of a NAND Flash memory cell. Each memory cell in the NAND architecture features a transistor with a control gate and a floating gate. To store information, a charge level is written to the cell by adding a specified amount of charge to the floating gate through Fowler-Nordheim tunneling by applying a relatively large voltage to the control gate [16].

To read a memory cell, the charge level written to the floating gate is detected by applying a specified word-line voltage to the control gate and measuring the transistor drain current. When reading a page, the same word-line voltage is applied to all cells in the page. The drain current is compared to a threshold by a sense amp comparator. If the drain current is above the comparator threshold, then the word-line voltage was sufficient to turn on the transistor, indicating that the charge written to the floating gate was insufficient to prevent the transistor from turning on. If the drain current is below the threshold, the charge added to the floating gate was sufficient

to prevent the applied word-line voltage from turning on the transistor. The sense amp comparator only provides one bit of information about the charge level present in the floating gate.

A bit error occurring at this threshold-comparison stage is called a *raw bit error* and we use the phrase *channel bit error probability* to refer to the probability of a raw bit error given a specified amount of distortion in the process of writing to the cell, retaining the charge level over a period of time, and reading the cell. We refer to this overall process as the *read channel*.

The word-line voltage or reference voltage required to turn on a particular transistor (called the threshold voltage) can vary from cell to cell for a variety of reasons. For example, the floating gate can be overcharged during the write operation, the floating gate can lose charge due to leakage in the retention period, or the floating gate can receive extra charge when nearby cells are written [17]. We refer to this variation of threshold voltage from its intended value as the *read channel noise*.

The probability density function of the read channel noise can be modeled by a Gaussian distribution. In this paper, we initially assume an i.i.d. Gaussian threshold voltage for each level of an SLC (i.e. two-level) Flash memory cell. This is equivalent to binary phase-shift keying (BPSK) with AWGN noise, except that the threshold voltage cannot be directly observed. Rather, at most one bit of information about the threshold voltage may be obtained by each cell read.

More precise models such as the model in [17] in which the lowest and highest threshold voltage distributions have a higher variance and the model in [18] in which the lowest threshold voltage (the one associated with zero charge level) is Gaussian and the other threshold voltages have Gaussian tails but a uniform central region are sometimes used. The model in [14] is similar to [18], but is derived by explicitly accounting for real dominating noise sources, such as inter-cell interference, program injection statistics, random telegraph noise and retention noise. After considering the simple Gaussian approximation for SLC, this paper considers MLC (4-level) Flash memory cells and uses the model of [14] to study the MMI approach and constant ratio method in a more realistic setting to complement the analysis using a simple i.i.d. Gaussian assumption.

B. Basics of LDPC codes

LDPC codes [19] are linear block codes defined by sparse parity-check matrices. By optimizing the degree distribution, it is well-known that LDPC codes can approach the capacity of an AWGN channel [4]. Several algorithms have been proposed to generate LDPC codes for a given degree distribution, such as the ACE algorithm [20], and the PEG algorithm [21].

In addition to their powerful error-correction capabilities, another appealing aspect of LDPC codes is the existence of low-complexity iterative algorithms used for decoding. These iterative decoding algorithms are called belief-propagation algorithms. Belief-propagation decoders commonly use soft reliability information about the received bits, which can

greatly improve performance. Conversely, a quantization of the received information which is too coarse can degrade the performance of an LDPC code.

Traditional algebraic codes, such as BCH codes, commonly use bounded-distance decoding and can correct up to a specified, fixed number of errors. Unlike these traditional codes, it can be difficult for LDPC codes to guarantee a specified number of correctable errors. However the average bit-error-rate performance can often outperform that of BCH codes in Gaussian noise.

The remainder of this paper studies how quantization during the read process affects the performance of LDPC decoding for Flash memory. In the next section, we present a general quantization approach for selecting word-line voltages for reading the Flash memory cells and apply it to the specific example of SLC (two-level) Flash using a simple Gaussian channel model.

III. SOFT INFORMATION VIA MULTIPLE CELL READS

Because the sense-amp comparator provides at most one bit of information about the threshold voltage (or equivalently about the amount of charge present in the floating gate), decoders for error control codes in Flash have historically used hard decisions on each bit.

A. Obtaining Soft Information

Soft information can be obtained in two ways: either by reading from the same sense-amp comparator multiple times with different word-line voltages (as is already done to read multi-level Flash cells) or by equipping a Flash cell with multiple sense-amp comparators on the bit line, which is essentially equivalent to replacing the sense amp comparator (a one-bit A/D converter) with a higher-precision A/D converter.

These two approaches are not completely interchangeable. The real goal is to detect soft information about the threshold voltage. Each additional read of a single sense amp comparator can provide additional useful information about the threshold voltage if the word-line voltages are well-chosen. In contrast, multiple comparators may not give much additional information if the drain current vs. word-line-voltage curve (the classic I-V transistor curve) is too nonlinear. If the drain current has saturated too low or too high, the outputs from more sense-amp comparators are not useful in establishing precisely how much charge is in the floating gate. If the word-line voltage and floating gate charge level place the transistor in the linear gain region, then some valuable soft information is provided by multiple sense amp comparators.

Our work focuses on the first technique described above in which soft information is obtained from multiple reads using the same sense-amp comparator with different word-line voltages.

This section investigates the potential improvement of increasing the resolution beyond one bit and studies how best to obtain this increased resolution. In [15], the use of soft information was explored and the poor performance of uniformly spaced word-line voltages was established.

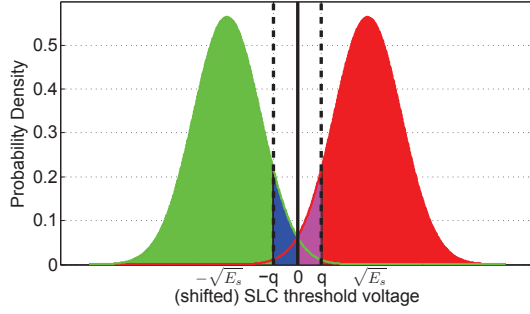


Fig. 2. Identically distributed Gaussian model for SLC threshold voltages. Also shown are word-line voltages for two reads (the dashed lines) and three reads (all three lines). The quantization regions are indicated by shading with the middle region for two reads being the union of the blue and purple regions.

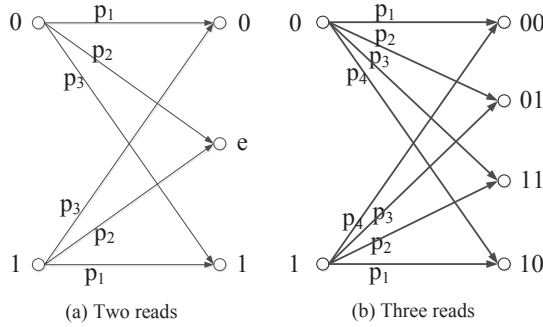


Fig. 3. Equivalent discrete memoryless channel models for SLC with (a) two reads and (b) three reads with distinct word-line voltages.

This paper takes an information-theoretic perspective on optimizing the word-line voltages. We study quantization models with different numbers of reads for both SLC (two-level) and MLC (four-level) Flash memories.

The fundamental approach of this paper is to choose the word-line voltages for each quantization by maximizing the MI between the input and output of each equivalent read channel. This approach has been taken in other work (not in the context of Flash memory) such as [11] [12]. Essentially, this paper seeks to quantize so as to create an effective read channel that has the maximum mutual information (MMI). Theoretically, this choice of word-line voltages maximizes the amount of information provided by the quantization. This section explores the simplest possible case, SLC (two-level) Flash using a Gaussian model.

B. Quantizing Flash to Maximize Mutual Information

This subsection describes how to select word-line voltages to achieve MMI in the context of a simple model of the two-level Flash cell read channel as BPSK transmission with Gaussian noise. The standard Flash system would use a single read. MMI word-line voltage selection is explicitly presented using two reads and three reads and the performance benefit is studied as a function of additional reads.

For SLC Flash memory, each cell can store one bit of information. Fig. 2 shows the model of the threshold voltage

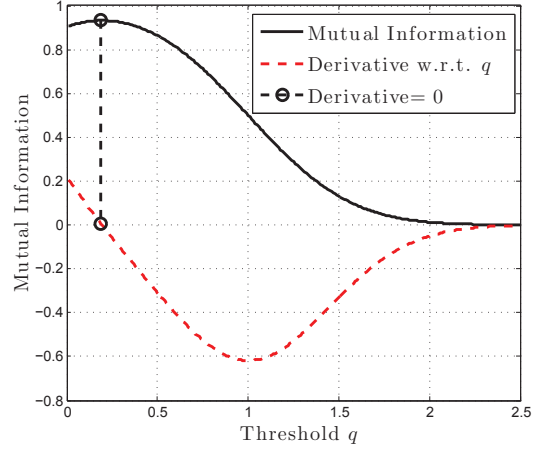


Fig. 4. MI vs. q (for $E_s = 1$) for $\text{SNR} = \frac{E_s}{N_0/2} = 7$ dB for SLC (two-level) Flash with two reads under the Gaussian model.

distribution as a mixture of two identically distributed Gaussian random variables. When either a “0” or “1” is written to the cell, the threshold voltage is modeled as a Gaussian random variable with variance $N_0/2$ and either mean $-\sqrt{E_s}$ (for “1”) or mean $+\sqrt{E_s}$ (for “0”).

1) *Two reads per cell*: For SLC with two reads using two different word-line voltages, which should be symmetric (shown as q and $-q$ in Fig. 2), the threshold voltage is quantized according to three regions shown in Fig. 2: the green region, the red region, and the union of the blue and purple regions (which essentially corresponds to an erasure). This quantization produces the effective discrete memoryless channel (DMC) model as shown in Fig. 3(a) with input $X \in \{0, 1\}$ and output $Y \in \{0, e, 1\}$.

Assuming X is equally likely to be 0 or 1, the MI $I(X; Y)$ between the input X and output Y of the resulting DMC can be calculated [22] as

$$I(X; Y) = H(Y) - H(Y|X) \\ = H\left(\frac{p_1+p_3}{2}, p_2, \frac{p_1+p_3}{2}\right) - H(p_1, p_2, p_3), \quad (1)$$

where H is the entropy function [22] and the relevant crossover probabilities shown in Fig. 3 (a) are $p_1 = 1 - Q^-$, $p_2 = Q^- - Q^+$, and $p_3 = Q^+$ with

$$Q^- = Q\left(\frac{\sqrt{E_s} - q}{\sqrt{N_0/2}}\right) \text{ and } Q^+ = Q\left(\frac{\sqrt{E_s} + q}{\sqrt{N_0/2}}\right), \quad (2)$$

where $Q(x) = \frac{1}{\sqrt{2\pi}} \int_x^\infty e^{-u^2/2} du$.

For fixed signal-to-noise ratio (SNR) $\frac{E_s}{N_0/2}$, the MI in (1) is a quasi-concave function of q and can be maximized numerically to find the parameter q that yields the MMI. Fig. 4 shows how MI varies as a function of q for an SNR of 7 dB. Note that when $q = 0$ there is no erasure region, which is equivalent to a single read. As q increases so does the erasure region. MI is concave in q between $q = 0$ and the point of inflection at $q = \sqrt{E_s} = 1$.

Because the MI is quasi-concave with a zero derivative only at the maximum MI and $q = \infty$, the optimal q in this case can be found by setting $dI/dq = 0$. Let $f(x)$ be the probability density function of a standard normal distribution. The derivative of the mutual information with respect to the threshold q is computed as

$$\frac{dI}{dq} = \sum_{j=1}^3 p_j'(q)(\log p_j(q) + 1) \quad (3)$$

$$= f(T_q^+) \log \frac{p_1 + p_3}{2p_3} + f(T_q^-) \log \frac{p_1 + p_3}{2p_1} \quad (4)$$

$$= f(T_q^+) \log \frac{1 + p_1/p_3}{2} + f(T_q^-) \log \frac{1 + p_3/p_1}{2}, \quad (5)$$

where $T_q^+ = \sqrt{E_s} + q$ and $T_q^- = \sqrt{E_s} - q$.

Note that dI/dq is continuous on \mathbb{R}^+ . At $q = 0$ we have $p_1 + p_3 = 1$. Applying this to (4), we have

$$\frac{dI}{dq} = -f(\sqrt{E_s}) \log 4p_1p_3 \geq 0, \quad (6)$$

at $q = 0$ by the inequality of arithmetic and geometric means. Equality holds only when $p_1 = p_3$. It can also be shown that dI/dq becomes negative for sufficiently large q and then increases monotonically with $\lim_{q \rightarrow \infty} g(q) = 0$. Together these properties (which are illustrated in the example of Fig. 4) ensure that there is a single zero derivative for finite q corresponding to the desired maximum MI. This optimum q can be found by an application of the bisection algorithm.

2) *Three reads per cell*: Now consider SLC with three reads for each cell. The word-line voltages should again be symmetric (shown as q , 0 , and $-q$ in Fig. 2). The threshold voltage is quantized according to the four differently shaded regions shown in Fig. 2. This quantization produces the DMC model as shown in Fig. 3(b) with input $X \in \{0, 1\}$ and output $Y \in \{00, 01, 10, 11\}$.

Assuming X is equally likely to be 0 or 1, the MI between the input and output of this DMC can be calculated as

$$\begin{aligned} I(X; Y) &= H(Y) - H(Y|X) \\ &= H\left(\frac{p_1 + p_4}{2}, \frac{p_2 + p_3}{2}, \frac{p_3 + p_2}{2}, \frac{p_4 + p_1}{2}\right) \\ &\quad - H(p_1, p_2, p_3, p_4), \end{aligned} \quad (7)$$

where the crossover probabilities are $p_1 = 1 - Q^-$, $p_2 = Q^- - Q^0$, $p_3 = Q^0 - Q^+$, and $p_4 = Q^+$ with Q^- and Q^+ as in (2) and

$$Q^0 = Q \left(\frac{\sqrt{E_s}}{\sqrt{N_0/2}} \right). \quad (8)$$

C. Performance vs. Number of Reads Per Cell

The MMI optimization approach generalizes to more reads per cell. Fig. 5 shows MI plotted against channel bit error probability for different numbers of reads per cell for the case of SLC. MI increases with the number of reads. The top (dashed) curve shows the MI possible with full soft information (where the receiver would know the threshold

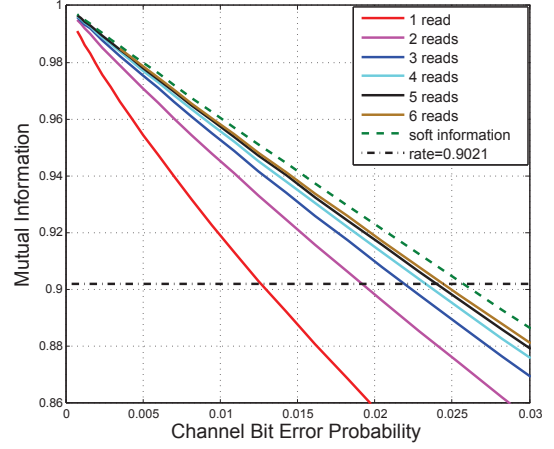


Fig. 5. MI provided by different quantizations for SLC (two-level Flash). The dashed horizontal line indicates the operating rate of our simulations. When an MI curve is below the dashed line, the read channel with that quantization cannot possibly support the attempted rate.

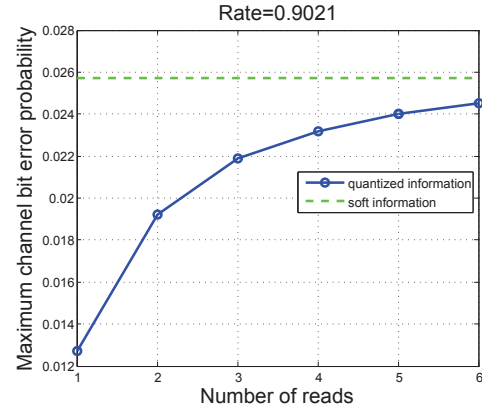


Fig. 6. Maximum tolerable channel bit error probability provided by different quantizations for SLC operating at rate 0.9021.

voltage exactly). The bottom curve shows the MI available with a single read. With two reads, the MI is improved enough to close about half of the gap between the single-read MI and the MI of full soft information. Increasing the number of reads improves the MI, but with diminishing returns as shown in Fig. 5.

Fig. 6 shows how the bit error probability requirement to achieve an MI of 0.9021 (the horizontal line in Fig. 5) increases (relaxes) as the number of reads increases.

Fig. 7 shows how the performance of an LDPC code (Code 2 described in Section IV below) improves as more soft information is made available to the decoder using MMI-optimized thresholds. This simulation uses the Gaussian model of the SLC Flash memory cell shown in Fig. 2. Fig. 7 plots FER versus channel bit error probability computed as $Q\left(\sqrt{\frac{2E_s}{N_0}}\right)$. For reference, the FER performance of a binary BCH code using one read per cell is also shown. Both the LDPC code and the BCH code have rate 0.9021. The LDPC code has a frame size of $k = 8225$ and the BCH code

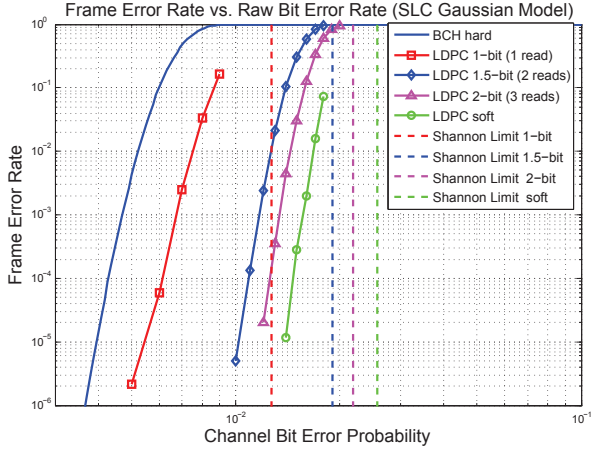


Fig. 7. Simulation results of FER vs. channel bit error probability using the Gaussian channel model for SLC (two-level) Flash comparing LDPC Code 2 with varying levels of soft information and a BCH code with hard decoding. Both codes have rate 0.9021. The BCH curve and the LDPC 1-read curve correspond to hard decoding.

has a frame size of $k = 8256$. Also for reference, dashed vertical lines show the Shannon limit (worst channel that could theoretically support reliable transmission) for each level of quantization at the target rate of 0.9021.

Consistent with the mutual information curves of Fig. 5, this plot illustrates that each additional read improves the FER performance of the LDPC code, but the performance improvement is diminishing. Three reads takes the LDPC code performance close to the limit of the performance achieved by that code with full soft information (essentially, an infinite number of reads). Note that the LDPC code outperforms the BCH code even with a single read, but one or two additional reads significantly improve performance.

IV. QUANTIZATION-BASED LDPC DESIGN TRADE-OFF

Because reading a page of bits from the sense-amp comparators is a time-intensive operation, it is likely that enhanced precision will be added progressively in actual implementations, and additional reads will only take place if needed to facilitate successful decoding. Hence, a single LDPC code will be decoded at a variety of precision levels. This introduces a design trade-off, which we will explore by comparing two LDPC codes.

Overall in this paper we consider three irregular LDPC codes, which we will refer to as Code 1, Code 2, and Code 3. The LDPC matrices¹ were constructed according to their respective degree distributions using the ACE algorithm [20], and the stopping-set check algorithm [23]. All of the simulations were performed using a sequential belief propagation decoder. The frame size is $k = 8225$ for each of the three LDPC codes.

The degree distributions of the three codes are as follows:

¹The complete LDPC code parity-check matrices are available at the CSL website <http://www.ee.ucla.edu/~csl/files/publications.html#COD>.

TABLE I
DENSITY EVOLUTION THRESHOLDS FOR THE THREE LDPC CODES STUDIED. THE AWGN DENSITY EVOLUTION THRESHOLD IS GIVEN BOTH IN TERMS OF σ AND $E_b/N_0 = -10 \log_{10}(2R\sigma^2)$ WHERE $R = 0.9021$. THE BSC THRESHOLD IS GIVEN IN TERMS OF THE CHANNEL BIT ERROR PROBABILITY ϵ .

| Code | Full-precision AWGN | | Single-Read AWGN | |
|------|---------------------|------------------|-----------------------|-----------------|
| | σ | $SNR = 2E_s/N_0$ | ϵ | $SNR(\epsilon)$ |
| 1 | 0.499 | 6.04 dB | 9.29×10^{-3} | 7.44 dB |
| 2 | 0.483 | 6.32 dB | 1.05×10^{-2} | 7.26 dB |
| 3 | 0.492 | 6.16 dB | 9.61×10^{-3} | 7.39 dB |

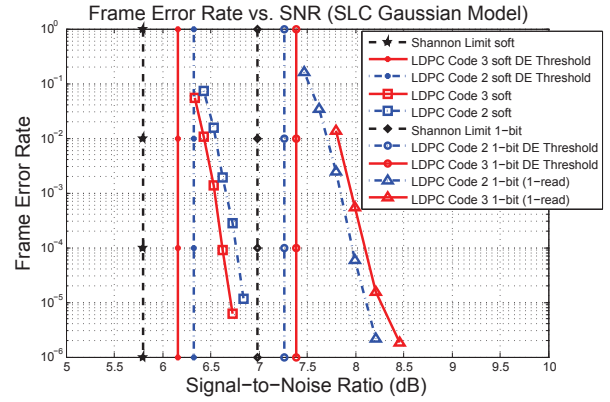


Fig. 8. Simulation results of FER vs. $SNR = 2E_s/N_0$ using the Gaussian channel model for SLC (two-level) Flash comparing LDPC Code 2 and LDPC Code 3 with hard decoding (1 read) and full soft decoding (essentially an infinite number of reads). Also shown are the Shannon limits for hard and soft decoding and the density evolution thresholds for the two codes under the two quantization scenarios. Both the density evolution results and simulation results show a trade-off between performance under hard decoding and performance under soft decoding.

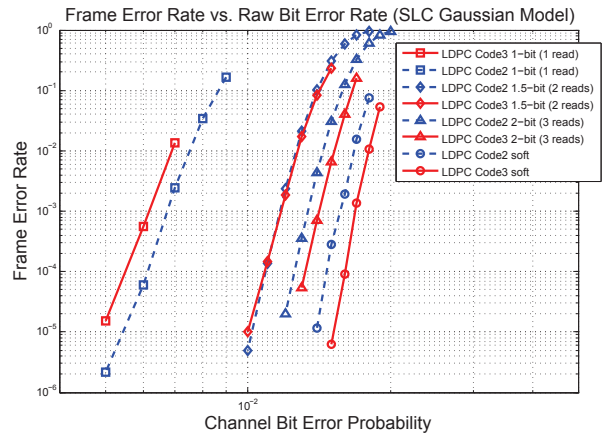


Fig. 9. FER vs. channel bit error probability simulation results using the Gaussian channel model for SLC comparing LDPC Codes 2 and 3 with varying levels of soft information and a BCH code with hard decoding. All codes have rate 0.9021. The BCH theory curve and the LDPC 1-read curve correspond to hard decoding.

$$\begin{aligned}\lambda_1(x) &= 2.0054 \times 10^{-5} + 3.5776 \times 10^{-2}x + 0.39869x^2 \\ &\quad + 8.4827 \times 10^{-3}x^8 + 3.7701 \times 10^{-2}x^9 + 0.51933x^{18} \\ \rho_1(x) &= 0.15662x^{54} + 0.84338x^{55}\end{aligned}$$

$$\begin{aligned}\lambda_2(x) &= 1.7701 \times 10^{-5} + 3.1579 \times 10^{-2}x + 0.46923x^3 \\ &\quad + 7.4877 \times 10^{-3}x^8 + 3.3278 \times 10^{-2}x^9 + 0.45841x^{18} \\ \rho_2(x) &= 1.0975 \times 10^{-3}x^{61} + 0.73267x^{62} + 0.26623x^{63}\end{aligned}$$

$$\begin{aligned}\lambda_3(x) &= 3.2172 \times 10^{-2}x + 2.681 \times 10^{-3}x^2 \\ &\quad + 0.55764x^3 + 0.40751x^{23} \\ \rho_3(x) &= 0.10366x^{57} + 0.89634x^{58},\end{aligned}$$

where $\lambda(x)$ is the left (variable-node) degree distribution and $\rho(x)$ is the right (check-node) degree distribution. A term of ax^{d-1} in $\lambda(x)$ indicates that a is the fraction of edges connecting to variable nodes with degree d .

Table I shows the density evolution thresholds for these three codes for the extremes of a full-precision SLC channel and a single-read SLC channel assuming the Gaussian model of Fig. 2.

Table I suggests that there is a trade-off between full precision performance and single-read performance. For example, Code 2 has a lower (in dB) single-read threshold than Code 3, but a higher full-precision threshold than Code 3. Fig. 8 shows FER vs. SNR simulation results consistent with the density evolution threshold results shown in Table I.

Fig. 9 compares the FER vs. channel BER performance curves for Codes 2 and 3 showing that for 2 reads the codes have essentially the same performance, but for three reads Code 3 has better performance.

An interesting area of future research is the development of codes that are “universal” across precision variations. It would be useful to design a code that can perform well over a large range of precisions or to show that such universal performance is not possible.

V. QUANTIZATION FOR MLC (4-LEVELS)

In this section, we extend the quantization approach to handle more than two levels, introduce a more realistic channel model, and present a method to reduce optimization complexity when there are more than two levels.

A. MMI Quantization for MLC

For MLC (4-level) Flash memory, each cell can store 2 bits of information. Figure 10 extends the previously introduced SLC Gaussian model in the natural way. Gray labeling (00, 01, 11, 10) minimizes the raw bit error rate for these four levels. Typically in 4-level MLC Flash, each cell is compared to 3 word-line voltages and thus the output of the comparator has 4 possible values (i.e., four distinct quantization regions).

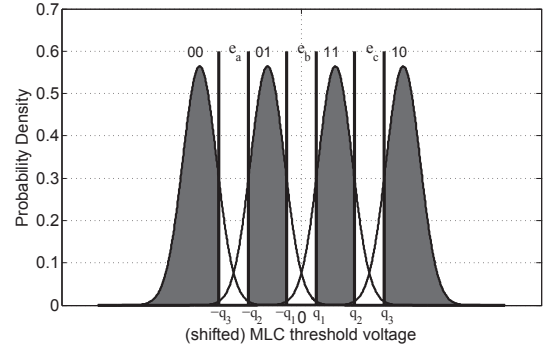


Fig. 10. Channel model for four-level MLC with threshold voltages modeled as Gaussians all sharing the same variance. Quantization is shown for six reads.

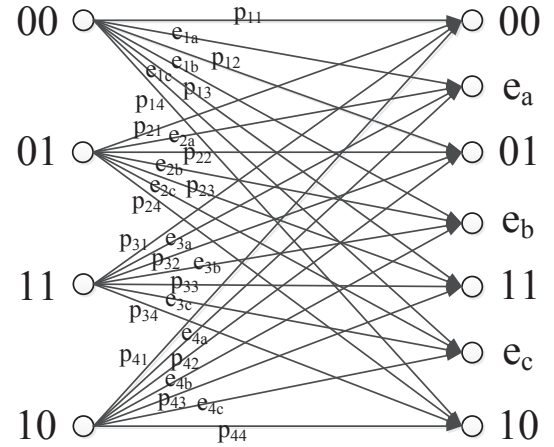


Fig. 11. Quantization model for 4-MLC with 6 reads.

If we consider three additional word-line voltages (for a total of six), the threshold voltage can be quantized to seven distinct regions as shown in Figure 10. The resulting DMC with four inputs and seven outputs is given in Figure 11. Since the channel is symmetric, the crossover probabilities for the channel model are symmetric in the upper and lower half of the figure, i.e., $p_{11} = p_{44}$, $e_{1a} = e_{4c}$, $p_{12} = p_{43}$, etc.

Similar to the SLC analysis, the MI between the input and output can be calculated as

$$\begin{aligned}I(X; Y) &= H(Y) - H(Y|X) \\ &= H\left(\frac{p_{11} + p_{21} + p_{24} + p_{14}}{4}, \frac{p_{12} + p_{22} + p_{23} + p_{13}}{4}, \right. \\ &\quad \left. \frac{p_{13} + p_{23} + p_{22} + p_{12}}{4}, \frac{p_{14} + p_{24} + p_{21} + p_{11}}{4}, \right. \\ &\quad \left. \frac{e_{1a} + e_{2a} + e_{2c} + e_{1c}}{4}, \frac{e_{1b} + e_{2b} + e_{2b} + e_{1b}}{4}, \right. \\ &\quad \left. \frac{e_{1c} + e_{2c} + e_{2a} + e_{1a}}{4}\right) \\ &\quad - \frac{1}{2}H(p_{11}, p_{12}, p_{13}, p_{14}, e_{1a}, e_{1b}, e_{1c}) \\ &\quad - \frac{1}{2}H(p_{21}, p_{22}, p_{23}, p_{24}, e_{2a}, e_{2b}, e_{2c}),\end{aligned}\quad (9)$$

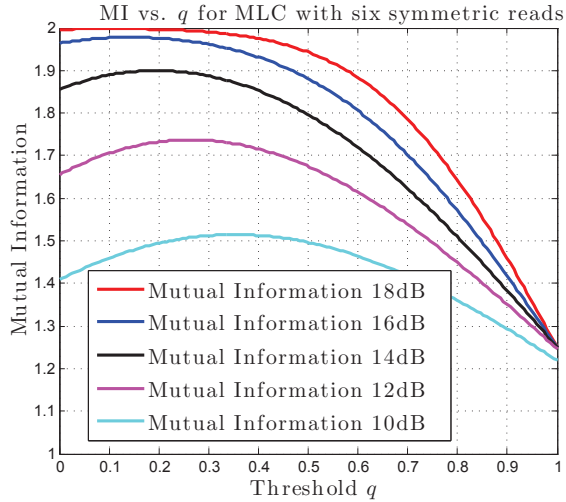


Fig. 12. MI vs. q for SNRs of 10, 12, 14, 16, and 18 dB for the Gaussian model of MLC (four-level) Flash with the symmetric thresholds $\mu_i \pm q$ for the four means $\{\mu_1, \mu_2, \mu_3, \mu_4\} = \{-3, -1, 1, 3\}$.

where all of the crossover probabilities can be calculated in the same manner as with SLC. Thus, in order to choose the optimal quantization levels $q_1, q_2,$ and q_3 for a fixed SNR, we maximize the MI given in equation (9).

This optimization becomes more cumbersome as the number of thresholds increases. The optimization problem is no longer quasi-concave unless carefully constrained. However, we were able to complete the optimization with three thresholds. We note that if the problem is constrained to a single parameter by selecting thresholds $\mu_i \pm q$ for the four equally spaced means $\mu_1 < \mu_2 < \mu_3 < \mu_4$, the problem becomes quasi-concave (or even concave) over the interesting region of $0 \leq q \leq \mu_i - \mu_{i-1}$ as shown in Fig. 12.

The qualitative behavior of MMI and required BER as the number of reads is increased in the MLC case is essentially the same as was shown in Figs. 5 and 6 for the SLC case.

Fig. 13 shows performance of unconstrained MMI quantization on the Gaussian channel model of Fig. 10 for 3 reads and for six reads for Codes 1 and 2. With four levels, three reads are required for hard decoding. For MLC (four-level) Flash, using six reads recovers more than half of the gap between hard decoding (three reads) and full soft-precision decoding. This is similar to the performance improvement seen for SLC (two-level) Flash when increasing from one read to two reads.

The two bits corresponding to a single MLC cell are actually associated with two distinct pages in many Flash implementations. However, with Gray labeling as in Fig. 10, the most significant bit can be ascertained with a single read (or the two central reads for enhanced precision as shown in Fig. 10) without performing the other reads. Similarly, the least significant bit using the labeling of Fig. 10 can be ascertained from the two outer edge reads (or four outer edge reads for enhanced precision as shown in Fig. 10) without performing the central read(s).

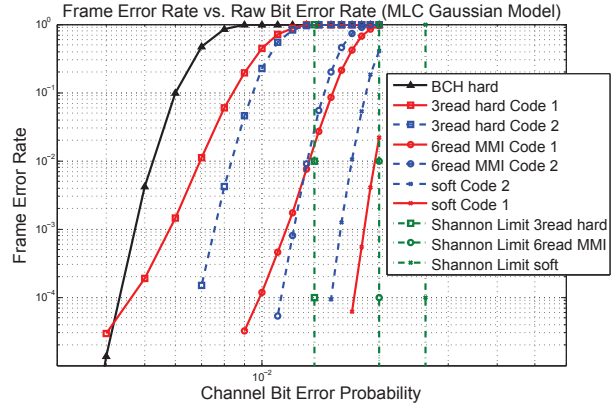


Fig. 13. FER vs. channel bit error probability simulation results using the Gaussian channel model for 4-level MLC comparing LDPC Codes 1 and 2 with varying levels of soft information and a BCH code with hard decoding. All codes have rate 0.9021. The BCH hard curve and the LDPC 3-read curves correspond to hard decoding.

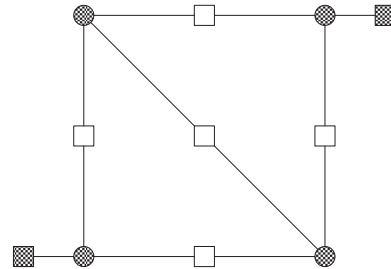


Fig. 14. A (4,2) absorbing set. Variable nodes are shown as black circles. Satisfied check nodes are shown as white squares. Unsatisfied check nodes are shown as black squares. Note that each of the four variable nodes has degree three. This absorbing set is avoided by precluding degree-3 nodes.

Because the read(s) associated with one of the two distinct bits turn out to be independent of the value of the other bit, the quantization optimization is not affected by whether the bits are stored in separate pages or not. However, it should be noted that with Gray labeling as in Fig. 10 the most significant bit enjoys a lower BER than the least significant bit for a given SNR. In our LDPC simulations, a single LDPC code included both the most significant bit and the least significant bit.

Note that in Fig. 13, the trade-off between performance with soft decoding and performance with hard decoding is even more pronounced. Code 1 is clearly superior with soft decoding but demonstrates a noticeable error floor when decoded with three or six reads.

LDPC error floors due to absorbing sets can be sensitive to the quantization precision, occurring at low precision but not high precision [24], [25]. Code 1 has small absorbing sets including the (4, 2), (5, 1), and (5, 2) absorbing sets. As shown in Fig. 14 for the (4,2) absorbing set, these absorbing sets can all be avoided by precluding degree-three variable nodes. Code 2 avoids these absorbing sets because it has no degree-3 variable node. As shown in Fig. 13, Code 2 avoids the error floor problems of Code 1.

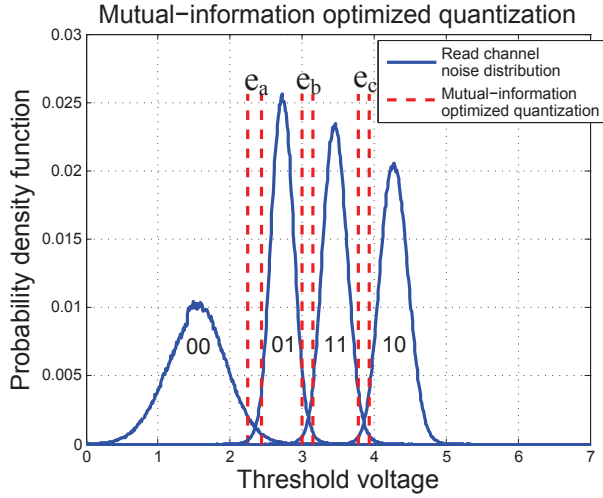


Fig. 15. Mutual-information optimized quantization for the 6-month data.

B. A More Realistic Model

We can extend the MMI analysis of Section III-B to any model for the Flash memory read channel. As an example, consider again the 4-level 6-read MLC as a 4-input 7-output discrete channel as shown in Fig. 11. However, instead of assuming Gaussian noise distributions as in Fig. 11, this subsection numerically computes the probability transition matrix using the retention noise model of [14] for a six-month retention period. Fig. 15 shows the four conditional threshold-voltage probability density functions generated according to [14] and the resulting six MMI word-line voltages that maximize MMI for this noise model. While the conditional noise for each transmitted (or written) threshold voltage is similar to that of a Gaussian, the variance of the conditional distributions varies greatly across the four possible threshold voltages. Note that the lowest threshold voltage has by far the largest variance.

Since the retention noise model is not symmetric, we need to numerically compute all the probabilities in Fig. 11 and calculate the MI between the input and output as shown in (10). The MI in (10) is in general not a quasi-concave function in terms of the word-line voltages q_1, q_2, \dots, q_6 , although it is quasi-concave for the simple model of two symmetric Gaussians with symmetric word-line voltages studied in [26]. Since (10) is a continuous and smooth function and locally quasi-concave in the range of our interest, we can numerically compute the MMI quantization levels with a careful use of bisection search.

C. The Constant-Ratio Method

In [15], a helpful heuristic constrains the additional word-line voltages to the left and right of each hard-decision word-line voltage so that the largest and second-largest conditional noise pdfs have a specified constant ratio R . This is a natural extension to general non-symmetric channels such as the one

$$\begin{aligned}
 I(X; Y) &= H(Y) - H(Y|X) \\
 &= H\left(\frac{p_{11} + p_{21} + p_{31} + p_{41}}{4}, \frac{p_{12} + p_{22} + p_{32} + p_{42}}{4}, \right. \\
 &\quad \left. \frac{p_{13} + p_{23} + p_{33} + p_{43}}{4}, \frac{p_{14} + p_{24} + p_{34} + p_{44}}{4}, \right. \\
 &\quad \left. \frac{e_{1a} + e_{2a} + e_{3a} + e_{4a}}{4}, \frac{e_{1b} + e_{2b} + e_{3b} + e_{4b}}{4}, \right. \\
 &\quad \left. \frac{e_{1c} + e_{2c} + e_{3c} + e_{4c}}{4}\right) \\
 &\quad - \frac{1}{4}H(p_{11}, p_{12}, p_{13}, p_{14}, e_{1a}, e_{1b}, e_{1c}) \\
 &\quad - \frac{1}{4}H(p_{21}, p_{22}, p_{23}, p_{24}, e_{2a}, e_{2b}, e_{2c}) \\
 &\quad - \frac{1}{4}H(p_{31}, p_{32}, p_{33}, p_{34}, e_{3a}, e_{3b}, e_{3c}) \\
 &\quad - \frac{1}{4}H(p_{41}, p_{42}, p_{43}, p_{44}, e_{4a}, e_{4b}, e_{4c}). \tag{10}
 \end{aligned}$$

shown in Fig. 15 of the constraint to a single parameter by selecting thresholds $\mu_i \pm q$ for the four equally spaced means $\mu_1 < \mu_2 < \mu_3 < \mu_4$ in the simple symmetric Gaussian model.

Note that the value of R at the natural hard-decision threshold is one because the two densities are equal. Higher values of R move these secondary thresholds further away from the hard decoding threshold. In Fig. 10 a higher value of R would correspond to larger “erasure” regions (shown in white). Although this heuristic is not named in [15], we will refer to it as the “constant-ratio” (CR) method.

In [15], the specification of R is left to empirical simulation. The CR method can be viewed as a constraint that can be applied to MMI optimization in order to reduce the search space.

The CR method can also simplify optimization because as with the symmetric constraint of Fig. 12 the MI is a quasi-concave function of R in the region of interest for the MLC (4-level) symmetric Gaussian channel. Fig. 16 shows MI as a function of R for MLC (four-level) Flash with six quantization thresholds (seven quantization levels) for both the simple symmetric Gaussian model and the more realistic retention model of [14]. The Gaussian and retention channels were selected so that they have an identical MMI for six-read (seven-level) unconstrained MMI optimization.

For both models the CR method with the MI-maximizing R provides essentially the same MI as obtained by the unconstrained MMI optimization. Furthermore, it is striking how similar the MMI vs. R behavior is for the two different channel models. For the Gaussian model, MI is a concave function of R . The curve of MI vs. R for the retention model closely follows the Gaussian model curve, but is not a strictly concave function because of variations in the numerical model.

The MMI approach is a way to select quantization levels in the hope of optimizing frame-error-rate (FER) performance. Fig. 16 shows the FER performance as a function of R for both the Gaussian model and the retention model for LDPC Code 2 described in Section IV below. The value of R that

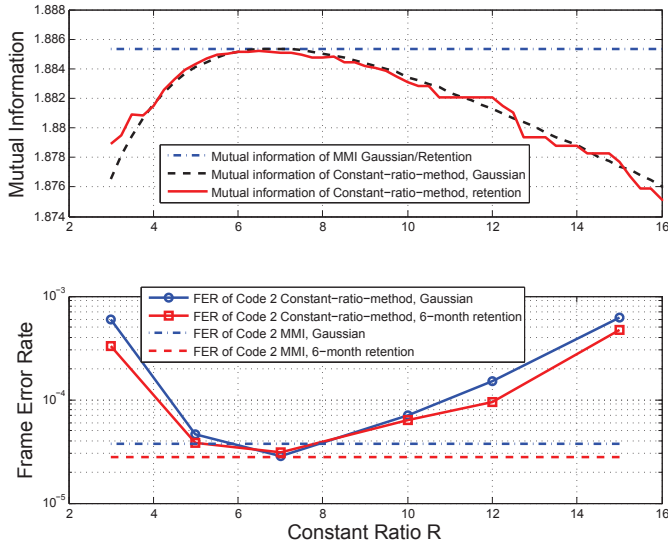


Fig. 16. Mutual information and frame error rate for Code 2 separately plotted as functions of the constant-ratio value R for six quantization thresholds (seven levels). Curves are shown for both the 4-PAM Gaussian model with SNR = 13.76 dB and the retention model of [14] for 6 months. These two models both have an MMI of 1.885 bits shown as a dashed line in the mutual information plot. The frame error rate plots are for LDPC Code 2 described in Section IV. The two models had slightly different frame error rates with MMI quantization, 3.78×10^{-5} for the 4-PAM Gaussian model and 2.8×10^{-5} for the retention model shown as dashed lines in the frame error rate plot.

provides the maximum MI also delivers the lowest FER as a function of R . This lends support to the approach of selecting quantization thresholds to maximize MMI.

Also, the constraint to a constant-ratio does not appear to adversely affect FER since the lowest FER as a function of R is essentially the same as (and in the Gaussian case even slightly better than) the FER achieved by unconstrained MMI quantization. The range of MI in Fig. 16 is small (approximately 0.01 bits), but this variation in MI corresponds to more than an order of magnitude of difference in FER performance.

D. MMI Optimization Thwarted by Small Absorbing Sets

While the previous example showed that optimizing MMI can also minimize FER for a well designed code, it is important to note that poorly designed codes can perform best with a quantization that does not maximize the channel mutual information.

To illustrate this, we previously introduced Code 1, which has a high error floor under hard decoding due to the presence of numerous small absorbing sets. As shown in Fig. 17, for Code 1, the lowest FER occurs with $R = 15$ which provides less mutual information than $R = 7$. This behavior may appear to be counter-intuitive. However, the numerous small absorbing sets serve as traps that can turn a few hard-decoded errors into uncorrectable problems. The presence of these absorbing sets forces the code to prefer a wider erasure region (thereby minimizing hard-decoded errors that trigger the absorbing sets) than would be optimal in terms of capacity.

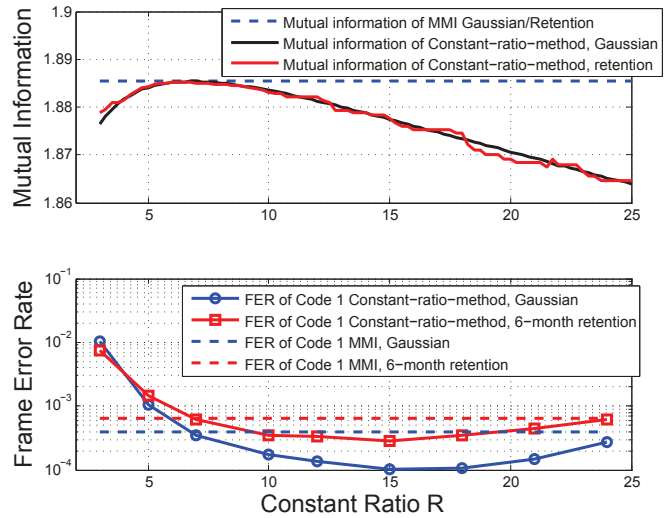


Fig. 17. Mutual information and frame error rate for Code 1 separately plotted as functions of the constant-ratio value R for six quantization thresholds (seven levels). Curves are shown for both the 4-PAM Gaussian model with SNR = 13.76 dB and the retention model of [14] for 6 months. These two models both have an MMI of 1.885 bits shown as a dashed line in the mutual information plot. The frame error rate plots are for LDPC Code 1 described in Section IV.

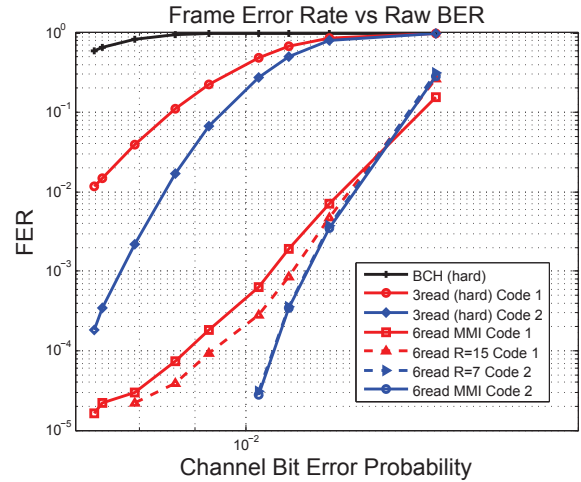


Fig. 18. FER vs. channel bit error probability results using the retention model of [14] for 4-level MLC. All codes have rate 0.9021. Hard decoding results are shown for the BCH code and LDPC Codes 1 and 2. FER performance for enhanced precision decoding using six reads is shown for LDPC Codes 1 and 2 using both unconstrained MMI quantization and MMI quantization with the constant-ratio constraint with the R value that minimizes FER for that LDPC code.

E. Simulation Results for Retention Model

Now we examine code performance using the retention model of [14]. Fig. 18 shows frame error rate (FER) plotted versus retention time for Codes 1 and 2 with three reads and with six reads.

The three-read quantization whose performance is shown in Fig. 18 is standard hard decoding for four-level MLC. We note that in principle, since the retention model is not symmetric, some gain can be achieved by allowing asymmetric thresholds and optimizing these thresholds using MMI even in the three-

read case. However, we found those gains to be insignificant in our simulations.

As in Fig. 13, Code 2 outperforms Code 1 under hard decoding in Fig. 18. For six reads, Code 2 still outperforms Code 1.

In Fig. 18, the Code-2 FER curves for unconstrained-MMI quantization and for $R = 7$ and indistinguishable. Note that $R = 7$ is both the MMI value of R and the value of R that empirically minimizes FER for Code 2. This was the hoped-for result of MMI optimization, that it would also optimize the true objective of minimizing FER. However, as we saw in Section V-D, if an LDPC code has a high error floor, optimizing the MMI does not necessarily minimize the FER.

Thus, a code with relatively poor performance can perform slightly better with a quantization that does not maximize the mutual information. Indeed, the best FER performance for Code 1 in Fig. 16 for six reads with constant ratio quantization is with $R = 15$. Note from Fig. 16 that $R = 15$ provides a smaller mutual information than $R = 7$, but $R = 15$ provided the lowest FER. Notice in Fig. 18 that for Code 1 with six reads, the MMI quantization performs slightly worse than the $R = 15$ quantization. Thus we can see that for a weaker code, the MMI approach may not provide the best possible quantization in terms of FER. However, this situation may well be interpreted as an indicator that it may be worth exploring further code design to improve the code.

VI. CONCLUSION

This paper explores the benefit of using soft information in an LDPC decoder for NAND Flash memory. Using a small amount of soft information improves the performance of LDPC codes significantly and demonstrates a clear performance advantage over conventional BCH codes.

In order to maximize the performance benefit of the soft information, we present an approach for optimizing word-line-voltage selection so that the resulting quantization maximizes the mutual information between the input and output of the equivalent read channel. This method can be applied to any channel model. Constraining the quantization using the constant-ratio method provides a significant simplification with no noticeable loss in performance. Furthermore, only a few additional reads can harvest most of the performance improvement available through enhanced precision.

Our simulation results suggest that if the LDPC code is well designed, the quantization that maximizes the mutual information will also minimize the frame error rate. However, we also saw that care must be taken to design the code to perform well in the quantized channel. An LDPC code designed for a full-precision Gaussian channel may perform poorly in the quantized setting, and the MMI approach does not lead to the lowest FER for a code with a high error floor.

REFERENCES

- [1] Y. Li, S. Lee, and et al. A 16 Gb 3b/cell NAND Flash Memory in 56nm With 8MB/s Write Rate. In *Proc. of ISSCC*, pages 506–632, Feb. 2008.
- [2] C. Trinh, N. Shibata, and et al. A 5.6MB/s 64 Gb 4b/Cell NAND Flash Memory in 43nm CMOS. In *Proc. of ISSCC*, page 246, Feb. 2009.
- [3] J.-D. Lee, S.-H. Hur, and J.-D. Choi. Effects of floating-gate interference on NAND flash memory cell operation. *IEEE Electron Device Letters*, 23(5):264–266, May 2002.
- [4] T. Richardson, M. Shokrollahi, and R. Urbanke. Design of capacity-approaching irregular low-density parity-check codes. *IEEE Trans. Inform. Theory*, 47(2):616–637, Feb. 2001.
- [5] E. Yaakobi, L. Grupp, P.H. Siegel, S. Swanson, and J.K. Wolf. Characterization and error-correcting codes for tlc flash memories. In *Computing, Networking and Communications (ICNC), 2012 International Conference on*, pages 486–491, 2012.
- [6] R. Gabrys, E. Yaakobi, and L. Dolecek. Graded bit error correcting codes with applications to flash memory. *IEEE Trans. Inform. Theory*, 59(4):2315–2327, Apr. 2013.
- [7] Fan Zhang, H.D. Pfister, and Anxiao Jiang. Ldpc codes for rank modulation in flash memories. In *Information Theory Proceedings (ISIT), 2010 IEEE International Symposium on*, pages 859–863, 2010.
- [8] Anxiao Jiang, M. Schwartz, and J. Bruck. Error-correcting codes for rank modulation. In *Information Theory, 2008. ISIT 2008. IEEE International Symposium on*, pages 1736–1740, 2008.
- [9] A. Mazumdar, A. Barg, and G. Zemor. Constructions of rank modulation codes. In *Information Theory Proceedings (ISIT), 2011 IEEE International Symposium on*, pages 869–873, 2011.
- [10] F. Sala, R. Gabrys, and L. Dolecek. Dynamic threshold schemes for multi-level non-volatile memories. *IEEE Trans. Comm*, 2013. to appear.
- [11] J. K.-S. Lee and J. Thorpe. Memory-Efficient Decoding of LDPC Codes. In *Proc. IEEE Int. Symp. on Info. Theory (ISIT)*, Adelaide, Australia, July 2005.
- [12] B. M. Kurkoski and H. Yagi. Quantization of Binary-Input Discrete Memoryless Channels, with Applications to LDPC Decoding. *Submitted to IEEE Trans. Inform. Theory*. Available <http://arxiv.org/abs/1107.5637>.
- [13] J. Bruck, A. Vardy, E. Yaakobi, J. Bruck, P.H. Siegel, A. Vardy, and J.K. Wolf. Storage coding for wear leveling in flash memories. In *Information Theory, 2009. ISIT 2009. IEEE International Symposium on*, pages 1229–1233, 2009.
- [14] Q. Wu, G. Dong, and T. Zhang. Exploiting Heat-Accelerated Flash Memory Wear-Out Recovery to Enable Self-Healing SSDs. In *USENIX Workshop on Hot Topics in Storage and File Systems (HotStorage)*, June 2011.
- [15] G. Dong, N. Xie, and T. Zhang. On the Use of Soft-Decision Error-Correcting Codes in NAND Flash Memory. *IEEE Trans. Circ. and Sys.*, 58(2):429–439, Feb. 2011.
- [16] R. Bez, E. Camerlenghi, A. Modelli, and A. Visconti. Introduction to Flash Memory. *Proc. IEEE*, 91(4), April 2003.
- [17] Y. Maeda and K. Haruhiko. Error Control Coding for Multilevel Cell Flash Memories Using Nonbinary Low-Density Parity-Check Codes. In *24th IEEE Int. Symp. on Defect and Fault Tolerance in VLSI Systems*, Chicago, IL, Oct. 2009.
- [18] S. Li and T. Zhang. Improving Multi-Level NAND Flash Memory Storage Reliability Using Concatenated BCH-TCM Coding. *IEEE Trans. VLSI Systems*, 18(10):1412–1420, Oct. 2010.
- [19] R. G. Gallager. *Low-Density Parity-Check Codes*. Cambridge, MA: MIT Press, 1963.
- [20] T. Tian, C. Jones, J. D. Villasenor, and R. D. Wesel. Selective Avoidance of Cycles in Irregular LDPC Code Construction. *IEEE Trans. Comm.*, 52(8):1242–1247, Aug. 2004.
- [21] X.-Y. Hu, E. Eleftheriou, and D.-M. Arnold. Progressive edge-growth Tanner graphs. In *Proc. IEEE GLOBECOM*, San Antonio, TX, Feb. 2001.
- [22] T. M. Cover and J. A. Thomas. *Elements of Information Theory, second Edition*. Wiley, Jul. 2006.
- [23] A. Ramamoorthy and R. D. Wesel. Construction of Short Block Length Irregular LDPC Codes. In *Proc. IEEE Int. Conf. on Comm. (ICC)*, Paris, France, June. 2004.
- [24] L. Dolecek, Z. Zhang, M. J. Wainwright, V. Anantharam, and B. Nikolic. Analysis of absorbing sets and fully absorbing sets of array-based LDPC codes. *IEEE Trans. Inform. Theory*, 56(1), Jan. 2010.
- [25] J. Wang, L. Dolecek, Z. Zahng, and R.D. Wesel. The Cycle Consistency Matrix Approach to LDPC Absorbing Sets in Separable Circulant-Based Codes. *submitted to IEEE Trans. Inform. Theory*. Available <http://arxiv.org/abs/1208.6094>, 2012.
- [26] J. Wang, T.A. Courtade, H. Shankar, and R.D. Wesel. Soft Information for LDPC Decoding in Flash: Mutual-Information Optimized Quantization. In *Proc. IEEE Global Telecomm. Conf. (GLOBECOM)*, Houston, TX, Dec. 2011.